Computer Simulation of the Interaction of Cu(I) with Cys Residues at the Binding Site of the Yeast Metallochaperone Cu(I)−Atx1

Sergio D. Dalosto[†]

Department of Physics, University of Washington, Seattle, Washington 98195-1560, and National Institute of Standards and Technology, Gaithersburg, Maryland 20899-8411

Received: October 11, 2006; In Final Form: January 4, 2007

The copper binding site and electronic structure of the metallochaperone protein Atx1 were investigated using the combination of quantum mechanics methods and molecular mechanics methods in the ONIOM(QM:MM) scheme at the density functional theory (DFT) B3LYP/ 6-31G(d):AMBER level. The residues in the binding site, −Met13−Thr14−Cys15−Cu(I)−Cys18−Gly17−Ser16−, were modeled with QM and the rest of the residues with MM. Our results indicate that the structure for Cu(I)−Atx1 has the copper atom coordinated to two sulfur atoms from Cys15 (2.110 Å) and Cys18 (2.141 Å) with an angle S−Cu(I) −S of 166°. The potential energy surface of the copper atom is used to estimate its binding energy and the force field for the copper ligands. The potential surface is shallow for the bending mode S−Cu−S, which explains the origin of the disorder observed in crystallographic and nuclear magnetic resonance studies. Using molecular dynamics for Cu(I)−Atx1 in a box of water molecules and in vacuum, with the force field derived in this work, we observed a correlated motion between the side chains of Thr14 and of Lys65 which enhances distortions in the S−Cu−S geometry. The results are compared with recent experiments and the previous models. The vibrational spectra for the copper ligands and for the residues in the binding site were computed. The localized modes for the copper ligands and the amide bands were assigned. The presence of the copper atom affects the amide bands' frequencies of the residues Cys15 and Cys18, giving resolved bands that can be used to sense changes in the binding site upon translocation of copper atom or interaction with target proteins. Furthermore, the EXAFS (extended X-ray absorption fine structure) spectrum of the proposed structure for Cu(I)−Atx1 was calculated and reproduced the experiments fairly well.

I. Introduction

Atx1 is a cytosolic yeast copper chaperone that delivers a copper atom to the transport ATPase *Ccc*2 in the trans-Golgi network. Atx1 has a human homolog, Atox1 and a bacterial homolog, CopZ. Atx1 proteins and their target ATPases have a conserved sequence −Thr−Cys−X−X−Cys− metal binding motif, with X representing any amino acid.[1−4] The metal (e.g., Cd, Hg, or Cu) is coordinated to the Cys residues and probably to an unknown weakly associated third ligand which may be from the binding site or may be exogenous. Several authors have discussed the mechanism for copper translocation from Atx1 to *Ccc*2 based on XAFS (X-ray absorption fine structure including EXAFS, extended X-ray absorption fine structure, and XANES, X-ray absorption near edge spectroscopy),[3] NMR (nuclear magnetic resonance),[5] genetic, and biochemical studies. These studies have shown that electrostatic, hydrogen bonding, and hydrophobic interactions between residues in the surface of Atx1 and *Ccc*2 guide the docking of both chaperons.[6,7] Thus, with the metal-binding site oriented towards *Ccc*2, an associative exchange mechanism biases the copper atom transfer.[3] Moreover, the translocation seems to occur in a reversible manner with a shallow thermodynamic gradient.[6] Nevertheless, the crystal structures of Cu(I)−Atx1 and Cu(I)−*Ccc*2 are still unknown. In particular, attempts to obtain the crystal structure of Cu(I)−Atx1 have been carried out but failed, mainly due to the disorder observed in the copper atom and the residues in the binding site.[8] Hence, the crystal structure of the oxidized apo and Hg(II) forms of Atx1 and some of its homologues are currently used to model the copper binding site in Atx1.

X-ray, NMR, and XAFS studies, independently or in combination,[5,9,10] have shed light on how the copper atom is coordinated in Atx1 and on the translocation mechanism between Atx1 and *Ccc*2. In particular, NMR studies have provided structural models for apo Atx1, Cu(I)−Atx1, and, in addition, information about the protein−protein interaction between Atx1 and *Ccc*2.[5,11,12] In spite of the important contribution of NMR to the metallochaperone−protein translocation mechanism and its structure, the structural arrangement of Cu(I)−ligands and the number of ligands cannot be observed experimentally. Instead, they have to be proposed indirectly. On the other hand, XAFS allows the study of the electronic structure of a copper atom and its environment but it requires a complementary structural model.[3,13] Although some models have been proposed for the Cu(I)−Atx1 structure, there is no consensus. Many details of the binding site remain unclear. For example, XAFS studies of Cu(I)−Atx1 have identified the first shell of ligands and the probable geometry around the copper. However, the proposed model is not conclusive since it includes two sulfur ligands (Cys15 and Cys18) from the Atx1 and an unknown third sulfur atom.

In order to put those proposals on a firm atomistic basis, it is important to have detailed first-principles calculations in combination with molecular mechanic methods such as the ONIOM-EE scheme (own N-layer integrated molecular orbital

[†] E-mal: sergio.dalosto@nist.gov.

10.1021/jp066689x CCC: $37.00
Published on Web 02/27/2007

SCHEME 1

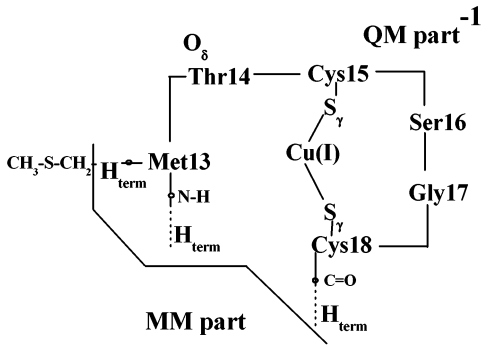

molecular mechanics-electronic embedding)[14] which can provide accurate information about the structure and binding energy of the copper atom in both Atx1 and *Ccc*2 chaperons. First-principles methods to model the active site of proteins combined with a classical force field for the rest of the protein are known to give reliable results for metalloproteins and other macromolecules.[15−18]

The goal of this work is to examine how the copper atom is coordinated in Atx1 and to shed some light on the copper atom translocation. To explore these issues, the copper atom and its surrounding residues in the binding site were modeled with first-principles methods while the steric and electrostatic contributions of the rest of the protein were modeled with molecular mechanics.

II. Methodology

The calculations were based on density functional theory for the quantum mechanics (QM) layer in combination with a molecular mechanics force field in the two-layer hydrogen link-atom scheme with the electronic embedding approach (ONIOM-EE) as implemented in Gaussian03.[14,19,20] Becke's three-parameter hybrid functional with the correlation functional of Lee, Yang, and Parr (B3LYP)[21] and the basis set 6-31G(d) for the QM layer and AMBER[22] force field were the level of theory used in this work.[14] The structure was considered to be relaxed when the forces in the QM part were less than 5×10^{-6} Eh Å^{-1}; the change of total energy at this time is typically less than 2×10^{-6} Eh. To simplify the computer effort during the minimization, different constraints in the MM layer were imposed for each model, as discussed below.

Structures. The computational models for Cu−Atx1 were based on the crystal structure of Hg(II)−Atx1 (Protein Data Bank or PDB accession number 1CC8) consisting of 72 amino acids. Because the first amino acid Met1 does not appear in the crystal structure, it was not included in this work. Since Met1 is far from the Cu binding site, it is expected to have a minor effect on the relaxed structure. The Hg atom in the Hg(II)−Atx1 structure was replaced by Cu and all the crystallographic water molecules were removed. No solvent effect was included in the ONIOM-EE calculations.[23] The protonation of the titratable residues was at pH 7. The QM layer consists of the residues Met13 (less its $-S-CH_3$), Thr14, Cys15, Ser16, Gly17, Cys18, and a copper atom. Met13 and Cys18 have the hydrogen link atom (H_{term}). Scheme 1 shows the residues included in the QM part and the H_{term} to link the QM part with the MM part. Because Met13 has a long side chain and part of it is buried in the MM layer, its side chain was replaced by $-CH_2-H_{term}$ and the $-S-CH_3-CH_{2-}$ was calculated as part of the MM layer. This cutoff did not change any of the results but accelerated the convergence. The total formal charge of the QM layer is −1, since Cys15 and Cys18 each have formal charge −1 and the Cu(I) has formal charge +1. The MM part has charge +2. Thus, the overall charge (QM + MM) is +1. During the relaxation, the QM layer is completely free to move whereas for the MM layer two different constraints were applied. In one case, the backbone of each amino acid was fixed; in the other, the whole MM layer was fixed. The structure for Cu(I)−Atx1 reported using NMR spectroscopy has the side chain of Cys18 (Cα−Cβ−Sγ) less exposed to the solvent than in the Hg(II)−Atx1 crystal structure. In addition, the S−Cu−S is (120° ± 40°) in the NMR structure. Thus, the geometry of the copper and the cysteines residues was changed to resemble the NMR structure. However, it was not possible to find a local minimum starting with that structure. These findings indicate that the NMR structure is not a good starting structure for ONIOM-EE calculations. See Figure S4 in the Supporting Information for an overlap of the crystal structure of Hg(II)−Atx1, and the one reported using NMR spectroscopy.

The apo−Atx1 model was based on the crystal structure of the apo−Atx1, PDB accession number 1CC7.[8] The QM layer comprised the residues Cys15 and Cys18 with two hydrogen atoms H_{term} for each residue as links to the rest of the protein as shown in Scheme S1 in the Supporting Information. The rest of the protein was modeled as an MM layer. During the relaxation, the backbone of atoms was fixed in position and only the side chain was allowed to relax. The crystal structure of the apo−Atx1 indicates the formation of a disulfide bridge between Cys15 and 18 with a distance of 2.0 Å between the sulfur atoms. The test calculations using the ONIOM-EE scheme reproduced that bridge fairly well yielding a bond distance of 2.10 Å.

To build a molecular force field for the copper atom and its ligands in Cu(I)−Atx1, the ESP charges (charges that fit the ElectroStatic Potential in a given surface) for the residues in the QM layer were calculated according to the Merz−Singh−Kollman Scheme[24] and the standard options in Gaussian03. A radius of 2.5 Å was used for the Cu atom and 1.75 Å was used for the S atom.

Molecular Mechanics parameters for Cu(I)−Atx1. Molecular mechanics methods are used intensively to study molecular dynamics, conformational energy searching, and docking in proteins.[25] They are based on a simple formulation of the local interactions, including harmonic bonds, angles, improper torsions, and dihedral angles. The potential-energy function for the copper atom in Atx1 chaperon was parametrized. The reference structure was the relaxed structure obtained using ONIOM-EE scheme and the potential energy surface (PES) was calculated in the rigid limit.[26] The copper and its ligands were displaced from the equilibrium along the bonds (Cu−Cys15Sγ, Cu−Cys18Sγ, Cβ−Sγ) and angles (Sγ−Cu−Sγ, in the plane and out the plane) as shown in Scheme S2 in the Supporting Information. The total energy was computed (including the QM and MM contributions in accordance with embedding scheme.[19] In Scheme S2 in the Supporting Information, the arrows show the direction of the displacements of the Cu atoms along the bonds and perpendicular to the bonds. The total energy curves vs bonds or angles were fitted and the corresponding MM field parameters were obtained using harmonic functions.[27] For example, Figure 1 shows the energy versus distance and the fitting for the Cu(I)−Sγ bond. The composed force constant is 202 and 206 kcal mol^{-1} Å^{-2} (1 calorie = 4.184 joules) for the Cu−Cys15 and the Cu−Cys18 bond, respectively. Then an average force constant for the bond Cu−Cys15S1 and Cu−Cys18S1 of 102

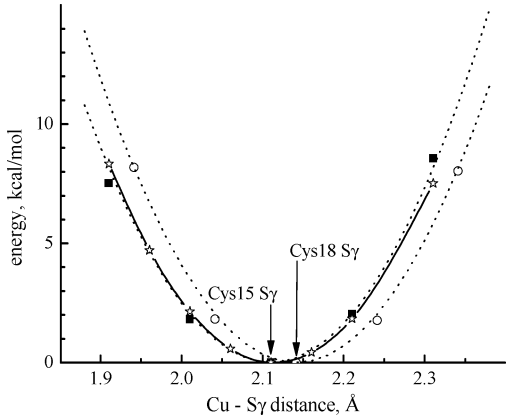

Figure 1. Cu−Cys15Sγ and Cu−Cys18Sγ distances vs energy obtained from ONIOM-EE calculations; full square symbols displacement along the bond Cu−Cys15Sγ and open circle symbols along Cu−Cys18Sγ. The dotted line is the result of least-squares fit using harmonic functions. The star symbol connected by a solid line is the molecular mechanic calculation.

kcal mol^{-1} Å^{-2} was calculated. The anharmonicity in this case was small and was neglected.

Molecular Dynamics. The simulation software for molecular dynamics (MD) was CHARMM and the force field was charmm22[28] with the addition of the parameters derived in this work. The MD of Cu(I)−Atx1 was carried out in a box of dimension (55 × 42 × 42) Å containing a total of 3096 explicit TIP3 water molecules[29] and, separately, in vacuum. In both simulations, the leapfrog Verlet integration scheme, the Berendsen constant temperature algorithm with coupling constant of 5 ps, and the SHAKE algorithm were used.[30] The simulations were performed at 300 K using a time step of 2 fs. The protein was gradually heated and then equilibrated over 200 ps and followed by run of 1 ns for the solvated protein and 200 ps in vacuum at constant temperature. In the MD simulation with water, the last 200 ps were used for analysis while in the vacuum simulation the last 70 ps were taken for analysis.

Vibrational Spectra. Vibrational spectroscopy gives information about the various functional groups present in a molecule. Hence, the vibrational spectra were calculated for the atoms in the QM layer in the ONIOM-EE approximation and also using the code CHARMM with the classical force field charmm22 and within Gaussian03 treating the whole Cu(I)−Atx1 as MM with Amber94 with the addition of the parameters derived in this work. The vibrational spectra shown in the text were generated with the calculated frequencies and intensities and with a Gaussian broadening of 15 cm^{-1}. Since the present work is focused in the copper binding site, only the bands corresponding to the atoms in the QM layer were assigned.

EXAFS calculations. The synergy between ONIOM-EE scheme, to model the structure of metalloproteins, and ab initio methods to calculate EXAFS spectra has recently been applied to decide among possible structures.[31] In addition, the Debye−Waller factors (DWFs), which depend on the correlation of atomic motion, can be calculated using local force constants based on classical force fields[32] or with ab initio methods.[33] We used the software package FEFF[34] (version 8.4) for the numerical simulation of the EXAFS spectra of the K absorption of the copper atom in the binding site of Atx1. This code uses a real-space multiple-scattering Green's function technique to simulate XAFS.[35] The local nature of EXAFS allows the neglect of atoms distant from the absorbing site, the copper in our case. Different structural models for Cu(I)−Atx1, based on the atoms in the QM layer in the relaxed structure proposed in this work, on the structure reported using NMR spectroscopy[12] (PDB accession number 1FD8), and 5 structures taken from the last 200 ps of molecular dynamics simulation were used as input for the EXAFS calculations. The energy-dependent exchange-correlation potential of Hedin and Lundqvist[36] was used for the fine structure and the atomic background. Heavy atoms (C, N, O) with similar environments were modeled with the same potential for the phase-shift calculation. Scheme S3 in the Supporting Information, shows the backbone of an amino acid with the corresponding indexes used in the calculations. For example, every C_α from the backbone has the same potential. Similarly, the same potential was used for all the hydrogen atoms.

To understand the contribution of the DWFs to the EXAFS spectra of Cu(I)−Atx1, two different methods implemented in the FEFF code were used to predict the DWFs.[32,34] The case study was for the structure proposed in this work. The methods used were the equation-of-motion method with the addition of the local force constants (stretching and bending) obtained in this work and from charmm22 and the correlated Debye model. The equation-of-motion method requires the computation of force constants to evaluate the DWFs corresponding to each path which was shown to improve the EXAFS spectra.[32] On the other hand, the simple correlated model uses a constant value for each path. The EXAFS calculated with these to models were compared (data not shown) and no significant improvement was observed with the use of the first model. Thus, in the EXFAS calculations reported in this work, the simple correlated model was used.[37] See the Supporting Information for the input file for FEFF calculations.

III. Results and Discussion

A. Proposed Structure for Cu(I)−Atx1. The structure of Cu(I)−Atx1 obtained using ONIOM-EE calculations is reported here and is compared to the crystal structure of Hg(II)−Atx1[8] and to the NMR structure of Cu(II)−Atx1. The relaxed structure of Cu(I)−Atx1 is presented in Figure 2 and a blow up of the binding site is shown in Figure 3. Since the backbones of the residues in the MM layer were fixed during the relaxation, the folding $\beta\alpha\beta\beta\alpha\beta$ is preserved. After the relaxation, the Cu(I) binding site is located in the surface of Atx1 and the Cu atom is coordinated to Cys15 (loop 1) and Cys18 (helix α1) in a linear arrangement similar to the one Hg(II) has in the crystal structure of Hg(II)−Atx1.[8] Table 1 lists some important distances for the proposed structure of Cu(I)−Atx1. For comparison, it also contains distances of the crystal structure Hg(II)−Atx1 and distances from the NMR spectroscopy of Cu(I)−Atx1. The amino moiety of Cys18 is close to the copper causing a steric interaction. It was observed in the crystal structure of Hg(II)−Atx1 that the side chain of Thr14 (Thr14−Oγ1) could be considered as a secondary bonding interaction of Hg(II) and the same role for Oγ1 in the Cu(I)−Atx1 structure was suggested.[8] However, in this work, it was found that for Cu(I)−Atx1, the oxygen Thr14−Oγ1 is 1.3 Å farther from the copper atom than it was observed for Hg(II), indicating a weak interaction between Oγ1 and Cu. Another residue close to the binding site is Lys65, which has formal charge +1 and was identified in the crystal structure of Hg(II)−Atx1. It was recognized that Lys65 is important for protein−protein interaction and recognition of *Ccc*2. Also, NMR studies suggested for Lys65 a role of protecting the binding site from solvent, oxidants or ligating atoms. But it is not clear what the contribution of Lys65 to the copper binding geometry is.[12] To better understand the contribution of Lys65 to the Cu(I) binding site, the relaxation

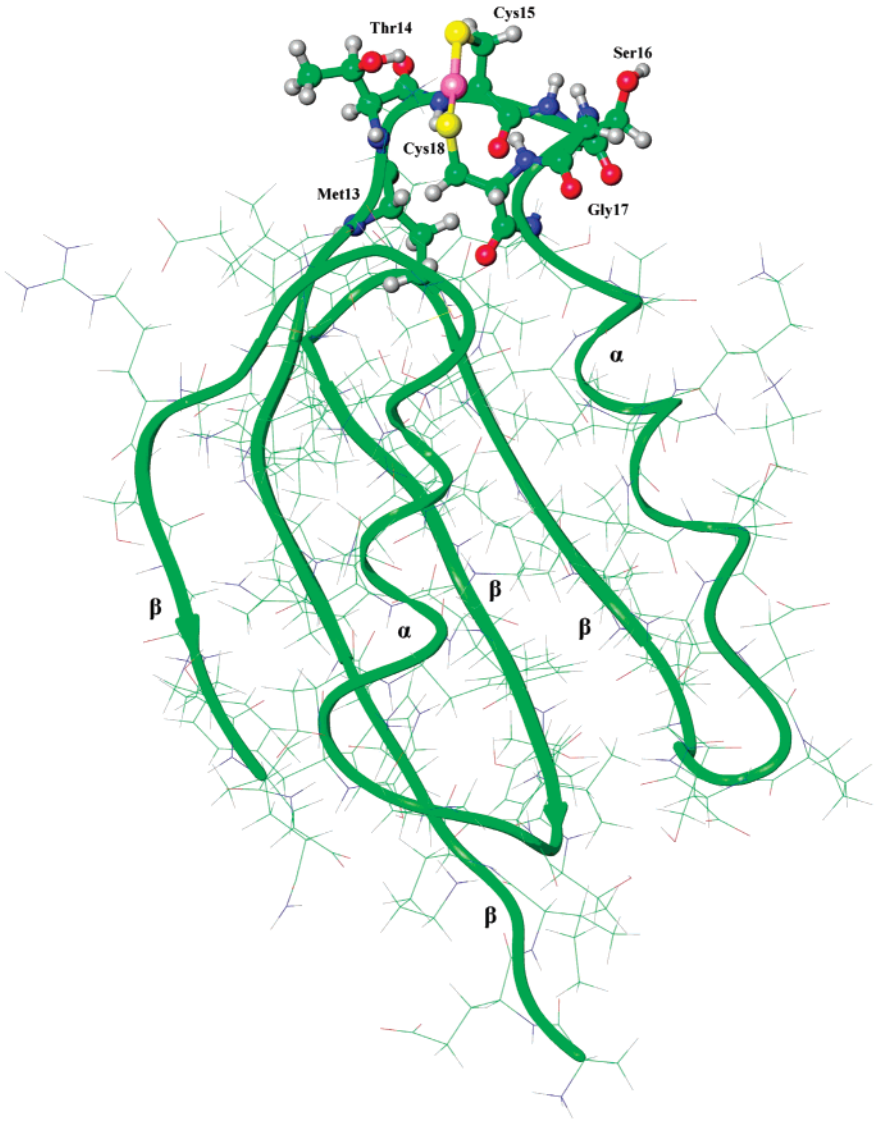

Figure 2. Cu−Atx1 metallochaperone. The Quantum Mechanics part is shown as tubes and balls while the Molecular Mechanics part is shown in wire frame. The folding $\beta\alpha\beta\beta\alpha\beta$ is indicated.

of the QM layer with the charges of the side chain of Lys65 equal to zero (Lys65^{neutral}) was carried out. (The MM layer was not allowed to relax). Since Lys65 is part of the MM layer, its contribution is primarily electrostatic. After the relaxation, small changes in the distances and overall geometry in the QM layer were observed. These changes seem to indicate that the role of Lys65 is more important for protein−protein recognition than for the Cu−Cys interaction. The Lys65Nζ−Cys18S distance is 3.98 Å, which can be compared to 3.22 Å obtained when Lys is charged, and to 3.91 Å observed experimentally in the crystal structure of Hg(II)−Atx1. The Thr14Oγ1 oxygen moves 0.5 Å toward the copper atom when Lys has charge zero. In addition, when the Lys65 is neutral, the ESP charges, which are sensitive to the electrostatic field surrounding a given atom, redistribute. With Lys65^{neutral} the ESP charges are 0.21*e*, −0.57*e*, and −0.62*e* for Cu, Cys18Sγ, and Cys15Sγ, respectively, resulting in a more symmetric charge density. See Table 2 for a comparison. Recently,[5] NMR spectroscopy showed that during the transient interaction, when the Cu(I)−Atx1 complex to the Ccc2a chaperone, the Lys65 takes a distant position from the binding site. This seems to allow the ligand-exchange reaction between the two chaperones.[38] Our results with Lys65^{neutral}, which is similar to having Lys65 far from the copper atom, suggest a role for Lys65 in controlling the electron charge density in the Cu(I)−ligands which could help the nucleophilic attack of Cys13 and Cys16 of Ccc2a. Moreover, Lys65 plays a roll in the Thr14 and the copper−ligand geometry and will be addressed in the subsection D using molecular dynamics.

So far, only one family and one minimized structure for Cu bound to Atx1 from NMR spectroscopy were reported.[12] These have provided hints to understand the metal capture and the release process better. As mentioned in the introduction, the Cu−ligands geometry and some residues in the binding site cannot be observed with NMR. Thus, the comparison between experimental NMR and the theoretical structure obtained with the ONIOM-EE scheme is important. The differences between the structure found in this work and that from NMR are significant. In the NMR structure the angle S−Cu−S is far from the linear geometry (120° ± 40°) suggesting the participation of another ligand, where as in our work that angle was found to be 166°. In the NMR structure, the bond Cβ−Sγ (Cys18) is oriented toward the binding site and buried in the solvent, but in the present work, the bond Cβ−SγCys18 is oriented out of the binding site. In consequence in our work, the bond Cβ−SγCys18 is exposed to the solvent. See Figure S4 in the Supporting Information for an overlap of the crystal structure of Hg(II)−Atx1, the NMR structure, and the structure proposed in the present paper. The orientation of the side chain of Thr14

TABLE 1: Some Distances Cu(I)−Residue in Å Taken from the Crystal Structure of Hg(II)−Atx1, NMR of Cu(I)−Atx1 and from This Work (ONIOM-EE and Average from MD Simulation)

residue−atom	Hg(II)−Atx1 X-ray, ref 8	Cu(I)−Atx1 NMR, ref 12	Cu(I)−Atx1 this work ONIOM-EE	Cu(I)−Atx1 this work MD vacuum/solvent
Thr14Oγ1	3.07	5.96	4.334	3.2 ± 0.2/3.1 ± 0.4
Thr14N	4.03	3.28	4.423	
Cys15Sγ	2.34	2.14	2.110	
Cys15N	3.26	2.11	3.342	
Cys15O	2.34	3.35	3.620	
Ser16Oγ	6.73	7.63	6.70	
Cys18Sγ	2.34	2.12	2.141	
Cys18N	3.13	4.23	3.083	
Lys65Nζ	5.18	3.31	4.714	3.6 ± 0.2/4.9 ± 0.7
Sγ−metal−Sγ	166°	120 ± 40°	166°	160° ± 6°/163° ± 5°

could not be detected in the NMR study. In our work, it is oriented towards the copper atom. Another difference concerns the position of the side chain of Lys65, which covers the binding site in the NMR study. In our work, Lys65 has less covering effect. These discrepancies will be discussed in more detail in subsection D using molecular dynamics, since Lys65 can have different conformations, whereas as the structure obtained with the ONIOM-EE method represents a static picture. Nevertheless, our Cu(I)−Atx1 structure is consistent with the family of possible structures reported using NMR.[11] Moreover, it seems to be a better model for the copper binding site than the minimized structure reported in ref 12.

B. Potential Surface of Cu for Cu(I)−Atx1. One of the causes for the failures in determining the crystal structure of Cu(I)−Atx1 is the presence of disorder in the copper binding site.[8] Also, NMR studies showed important fluctuation in the residues around the copper atom.[5] With this motivation, the potential surface of copper was studied using the ONIOM-EE scheme. The resulting potential surface is shown in Figure S1 in the Supporting Information. The curve along the S−Cu bond in Figure S1 in the Supporting Information is similar to the one showed in Figure 1 with open circle symbols. The thick dashed line indicates the isoenergy surface with energy ≈1 kT (T = 298.0 K).[39] The extreme in this isoenergy surface corresponds to an angular spread of ≈18° (0.36 Å) and a change in the distance along the bond of ≈0.12 Å. The potential surface is shallow along the bending S−Cu−S and indicates the possible source of disorder reported for the crystal structure and NMR. The potential surface for displacement of the copper atom in the direction perpendicular to the plane S−Cu−S is also shallow

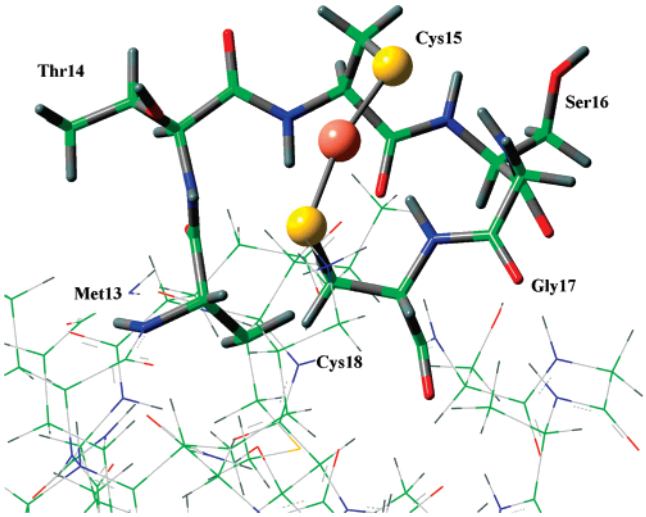

Figure 3. Detail of the coordinated copper atom (pink) and the ligands Cys15 and Cys18 with sulfur atoms in yellow.

TABLE 2: Ideal Bond Distances, Stretching Force Constants (K_b), Ideal Valence Angles, Angle-Bending Force Constants (K_θ), and Charges Obtained from QMMM Calculations for Cu(I)−Atx1[a]

bond	K_b (kcal mol^{-1} Å^{-2})	R_0 (Å)
Cu(I)−Cys15Sγ	102	2.110
Cu(I)−Cys18Sγ	102	2.141
Cys15 | Cβ−Sγ	100	1.847
Cys18 | Cβ−Sγ	100	1.868
angle	**K_q (kcal mol^{-1} rad^{-2})**	**(deg)**
Sγ−Cu−Sγ	40	166°
Cβ−Sγ−Cu	35	100°
charges		
	Merz−Kollman	Mulliken
Cu	0.31	0.074
Cys15 | Sγ	−0.58	−0.34
Cys15 | Cα	−0.19	
Cys15 | Cβ	0.03	
Cys18 | Sγ	−0.83	−0.53
Cys18 | Cα	−0.10	
Cys18 | Cβ	0.14	
van der Waals data taken from ref 49		
	R_{min} (Å)	E_{min} (kcal/mol)
Cu	1.09	0.25

[a] These parameters may be used in AMBER or CHARMM force field calculations (1 cal = 4.184 J).

and some anharmonicity is observed (data not shown). These findings give a hint of the mechanism for Cu release and the expected disorder for the binding site.

C. Force Field Parameters Derived for Cu(I)−Atx1. There has been success in modeling different properties of metalloproteins using classical force fields.[25] In many cases, the force field parameters for the metal and its ligands are specific for the system under study. These Molecular Mechanics parameters are reliable if they can reproduce the conformational and dynamical behavior and vibrational frequencies for a given system. Table 2 shows the ideal bond distances and the parameters derived in this work, as explained in Section II. The parameters are specifically for the Cu and S and Cβ of Cys15 and Cys18. The rest of the force field used is taken from AMBER or charmm22 force fields without any change. These parameters reproduce the structure and the vibrational frequencies fairly well computed with ONIOM-EE method presented in the previous subsection.

Next, a molecular dynamics study allowed the study of the stability of the structure of Cu(I)−Atx1 with the force field parameters derived in this work and the calculation of some important statistical quantities.

D. Molecular Dynamics. The ONIOM-EE computations of subsection A indicated how the copper atom interacts with the residues in the binding site and allowed the force field parameters to be obtained. However, these calculations were performed with constraints in the MM layer and represent a static structure for Cu−Atx1. Due to these limitations, the effects of dynamics of the structure and the steric and electrostatic effects of the rest of the protein environment during dynamics could not be explored. In addition, no solvent effect was taken into account. Thus, a 1 ns molecular dynamics study of Cu(I)−Atx1 in a box of water molecules and in vacuum was carried out. The time evolution of the distances between copper and the residues Thr14Oγ1−Cu and Lys65Nζ-Cu in the binding site and the angle (S−Cu−S) during the simulations of the solvated Cu(I)−Atx1 are presented in Figure S2 in the Supporting Information and in Table 1.

In vacuum, a concerted motion of the Thr14O γ1 and Lys65Nζ was observed, followed by a distortion in the S−Cu−S geometry, as anticipated with the ONIOM-EE calculations. When the Oγ1 and the Cu move closer (i.e., S−Cu−S angle decreases), Lys65 moves away from the active site. This concerted motion is interesting because it has implications for the translocation process. To further study these events, Cu(I)−Atx1 was solvated in a box of water molecules; see section II for details. The concerted motion observed in vacuum does not occur in the solvated study. This is due to the screening created by the water molecules to the interaction between Oγ1, Cu, and Nζ. However, Lys65 and Thr14 have an increase in the fluctuations around their equilibrium positions with respect to the vacuum simulation (data not shown). The presence of water screens the interaction between Lys65 and Cys15S−Cu−CysS18 and Thr15Oγ. This suggests adjusting the charges in the binding site to be used during the MD simulation to a situation where the charge on the Cys15S-Cu−CysS18 is more symmetric. Interesting, in the C-terminus of human HAH1, upon Cu(I) binding, the side chain of Lys60 residue move toward metal suggesting a common characteristic.[40]

These findings agree with the NMR study[12] in which fluctuating residues are inferred from the experiments. The molecular dynamic simulation of the solvated Cu(I)−Atx1 shows some water molecules interacting with the Thr and Lys. At least one water molecule makes a link between Cu and Thr and remains interacting with Thr and Cu during the simulation.

Some important questions remain such as the solvent's access to the binding site and the role of Lys65 in the solvent's accessibility. Nevertheless, I believe that the structure for the metallochaperone Cu(I)−Atx1 proposed in this work captures some of the essential aspects of the copper binding in Atx1.

E. Vibrational Frequencies for the Copper Atom and the Residues in Binding Site. Vibrational spectroscopy gives information about various functional groups present in proteins and how they interact with the surroundings.[41,42] For example, the amide I and III spectral bands have been used successfully for secondary structure analyses. The amide I band results from the C═O stretching vibration of the amide group coupled to the bending of the N−H bond and the stretching of the C−N bond. These infrared vibrations have a strong signal and are between 1600 cm^{-1} and 1700 cm^{-1}, but they have interference from water vibrational bands, and overlap with other protein vibrations. On the other hand, the amide III bands (1350−1200) cm^{-1} have a weak signal but they do not have the same interferences which amide I bands have.[43] It is interesting to calculate the vibrational frequencies involving the copper and its ligands to determine the importance of the strength of the Cu(I)−S bond in controlling the translocation of copper from Atx1 to *Ccc*2. With this motivation, the vibrational spectra in the range (10 to 3500) cm^{-1} were calculated using ONIOM-EE and the classical force field AMBER (given in parenthesis) with the incorporation of the parameters derived in this work, and the bands were assigned.

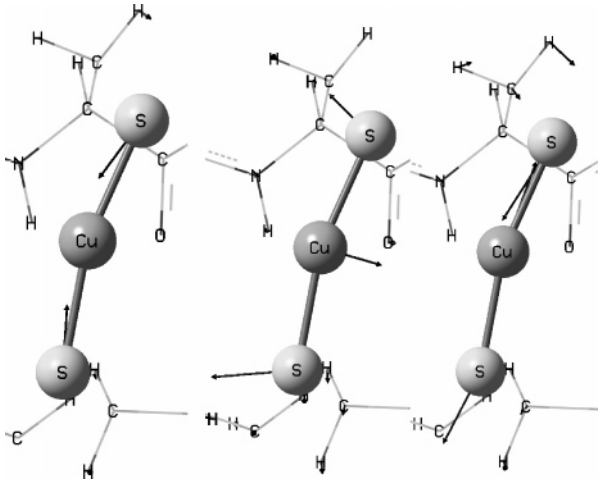

Figure 4. Calculated mode of vibration in Cu(I)−Atx1. From left to the right, symmetric, bending and asymmetric modes. The arrows indicate the direction of the displacement.

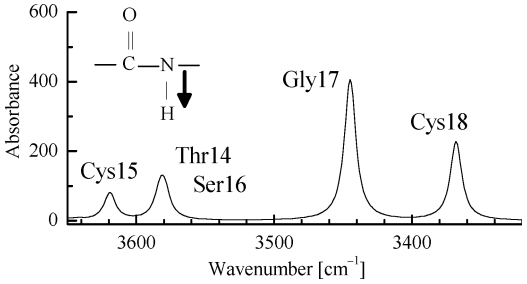

Figure 5. Calculated amide A band of Cu(I)−Atx1. The arrow indicates the direction of the displacement. The labels indicate the residues involved in each band. Absorbance is in arbitrary units.

The bands corresponding to the localized vibrational mode of the S−Cu−S are shown in Figure 4. These calculated vibrational modes are in the THz region. $\nu_a = 373$ cm^{-1} (383 cm^{-1}) corresponds to the asymmetric mode, $\nu_b = 127$ cm^{-1} (162 cm^{-1}) corresponds to the bending mode, and $\nu_s = 303$ cm^{-1} (288 cm^{-1}) corresponds to the symmetric mode. There is no experimental information available for comparison; however, it is anticipated the deviation is not greater than 10%. The ratio of intensities is (ν_a:ν_b:ν_s) 6:1:3. Compared with the intensities of the calculated amide I bands, presented below, the localized S−Cu−S mode ν_b has an intensity 80 times weaker.

Next, the amide (I, II, and A) bands for the residues in the QM layer of Cu(I)−Atx1 are reported. The amide A band is shown in Figure 5, and the peaks are labeled with the corresponding residues. The residues −Met13−Thr14−Cys15− are in the loop 1 and −Ser16−Gly17−Cys18− in the beginning of the helix α1. The frequencies of the amide A bands decrease from Met13 to Cys18 as the residues becomes to be more α helix. This result is consistent with experimental studies in other proteins.

The amide I and II bands are shown in Figure 6. The amide I peak centered at 1688 cm^{-1} corresponds to the collective vibration of the residues in the binding site. The residues Cys15 and Cys18 also have resolved bands. Resolved bands are also observed in the amide II spectral region for Cys15 and Cys18.

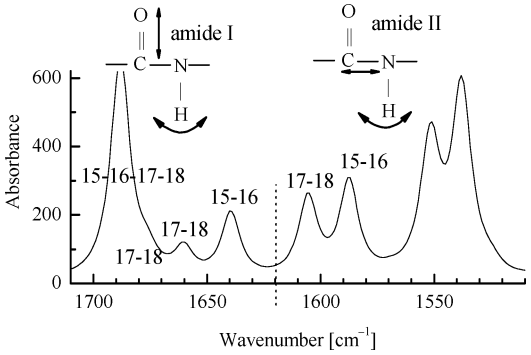

Figure 6. Calculated amide I and II band of Cu(I)−Atx1. The arrow indicates the direction of the displacement. The numbers indicate the residue involved in the band. The label15−16, for example, means $(C{=}O)_{15}$ and $(N{-}H)_{16}$. Absorbance is in arbitrary units.

The explanation of these resolved bands is the interaction, which is through-space (electrostatic) and through-bond covalent of the copper atom with Cys15 and with Cys18.

The resolved bands reported here might overlap with other protein bands and thus be hard to detect. However, if these bands were resolved in an experiment, then they could be used to detect changes in the binding site upon docking with a target protein or with exogenous ligands. I speculate that when the copper atom is released, the bands should shift to the most populated frequencies. For example, the amide I band labeled as 15−16 and 17−18 should move toward the peak labeled as 15−16−17−18 in Figure 6. The amide III bands are not shown in this work because they were difficult to assign as they are weak and are mixed with other vibrations.

The computed vibrational frequencies showed an interesting feature; however, they were done without solvent, i.e., in vacuum. It is likely that the amide I and A bands' frequencies are lower when solvent is present due to a hydrogen bond interaction or due to a dielectric effect. However, I expect they maintain their relative positions.

F. XANES and EXAFS Spectrum of the Cu(I)−Atx1 Structure. A major problem in any computational prediction is its validation.[44] Usually, in order to validate structural models, the IR bands, UV−vis, CD (circular dicroism), NMR spectra are calculated and then compared with experiments. In this work, the EXAFS spectrum was used to further validate the Cu(I)−Atx1 structure proposed in this work. EXAFS experiments are abundant and comprise different Cu(I) metallochaperones with similar binding site than Atx1, such as Atox1, WND and MNK.[13] From the simulation of the experimental EXAFS spectrum it was found[3] that the copper is Cu(I) and is coordinated to two sulfur ligands at 2.25 Å. But the need for a unknown third ligand at 2.4 Å was suggested in order to improve the simulation.[3] It is not clear whether the third ligand comes from the binding site or if it is an exogenous thiol. It was shown experimentally that Atox1 and the N-terminal domain of the ATP7B Wilson disease protein bind to the exogenous DTT (dithiothreitol).[45] But the origin and its possible role in metallochaperones function are unclear. The third ligand is still invoked in the EXAFS studies of HAH1, even if the thiols are excluded during its preparation.[13,46] However, I would like to understand the contribution of neighboring atoms of the copper in the binding site to the EXAFS spectrum better. The spectrum probably could be explained only invoking the surrounding residues of copper. To pursue the calculation of the EXAFS spectrum, the structure for Cu(I)−Atx1 proposed in this work using ONIOM-EE methods as well as, structures taken from the MD simulation and from NMR[12] were used.

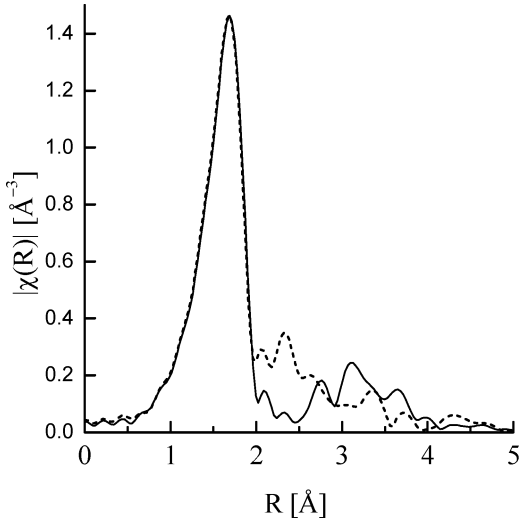

Figure 7. Radial distribution function derived from the calculated EXAFS spectra of Cu K-edge of Cu(I)−Atx1, solid line using the structure obtained with ONIOM-EE calculations, dotted using NMR structure (ref 12).

The Cu XANES and EXFAS spectrum of Cu(I)−Atx1 were reported in ref 3. In particular the XANES spectrum shows the characteristic pre-edge feature at 8984 eV of Cu(I) (see Figure 2A,B of ref 3). The weak shoulder corresponds to the copper 1s → 4p transition.[47,48] The intensity and shape of the peak depend on the symmetry of the Cu and its ligands, given that the 4p (p_x, p_y and p_z) orbital has different splitting. The ONIOM-EE calculation of Cu(I)−Atx1 shows the Cu−ligands with C_1 symmetry, so the 4p orbitals have different energy. Scheme S4 in the Supporting Information, shows the molecular orbital diagram obtained from the ONIOM-EE calculations. The 1s orbital of Cu(I) is the first occupied orbital. The 4p orbitals of copper are above the HOMO (highest occupied molecular orbital) orbital and the p_x, p_y, and p_z states have different energies. The electronic structure of Cu(I)−Atx1 was analyzed using ONIOM-EE methods to understand the contribution of the highest occupied orbitals to the binding of copper atom. The HOMO has contributions from the Cu−$3d_{zx}$ orbital (16%) and S-p (32%) of sulfur ligands, while the second highest occupied molecular orbital has a 16% Cu−$3d_{z^2}$ and a 32% S-p contribution.

Figure 7 shows the EXAFS spectra calculated using the ONIOM-EE and the NMR structures (which can be compared with Figure 2B of ref 3). They are similar in the (0 to 2) Å region which corresponds to the Cu−Cys15S and Cu−Cys18S paths and differ considerably beyond 2 Å. The atoms contributing to the region beyond 2 Å belong to the residues Cys15 and Cys18. The most interesting source of structural information in the spectrum is between 2 Å and 4 Å. In the NMR structure Cys15 is closer to the Cu(I) than Cys18 giving an important contribution to the spectra between 2 Å and 3 Å. While in the structure proposed in the present paper the signal between 2 Å and 3 Å reproduce better the experimental spectra (see Figures 2 A and B of ref 3). Since the structures used here represent static structures for Cu(I)−Atx1, 5 structures taken from the MD simulations, Figure S3 in the Supporting Information, were used to prepare structural models for EXAFS calculations which are shown in Figure 8. The structures presented in Figure S3 in the Supporting Information show the typical fluctuations during the MD simulation. The spectra, Figure 8, are similar between (0 to 2) Å, with the exception of the spectrum for 80 ps which has Cu−Cys18S = 2.28 Å, far from the average value. Beyond

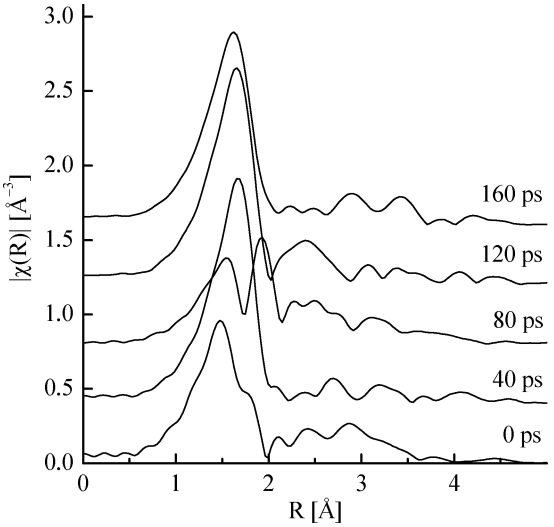

Figure 8. Theoretical radial distribution function derived from the EXAFS spectra of Cu(I)−Atx1 calculated using the 5 structures taken from the last 200 ps molecular dynamic simulation. The time indicated in the figure corresponds to the one indicated by star symbols in figure S4 in the Supporting Information. The spectra were displaced by 0.4 units along the *y*-axis.

2 Å, the peaks have contributions from both Cys15 and Cys18 and less from the other surrounding amino acids. A careful study of the shell beyond 2 Å could give rich structural details around the copper and the surrounding amino acids.

Although we obtain good agreement between experiments and the computed EXAFS spectrum using the ONIOM-EE structure, these calculations seem to indicate that any of the surrounding atoms of the copper, except the two sulfur atoms, could be the third scattering atom invoked in ref 3.

IV. Summary

The metallochaperone Atx1 transports copper into a specific intracellular location and translocates the copper to a specific target (Ccca2). The structure of the binding site of copper and the surrounding amino acids in Atx1 is relevant to understand the details of translocation mechanism better.

I used first-principles density-functional calculations in combination with Molecular Mechanics to predict the structure of the metallochaperone Cu(I)−Atx1. The calculations indicate a structure similar to Hg(II)−Atx1. Besides, the proposed structure could belong to the family of structures reported using NMR spectroscopy, and is a better model than the average structure obtained from that family. The copper is coordinated to two sulfur atoms of Cys15 and Cys18 in a nearly linear arrangement and is exposed to the solvent. The potential surface of copper is shallow for the bending mode, which explains the source of disorder detected in the crystallographic and NMR studies. Both static and molecular dynamics calculations show that the side chains of Thr$O\gamma 1$ and Lys65Nζ have a correlated motion that affect the S−Cu−S geometry. I speculate that mutating the Thr14 for other residue may reduce the motion of the copper and the disorder in the surrounding amino acids facilitating the resolution of a crystallographic study. Of course, there are many limitations of the theoretical analysis, and the real situation could be much more complicated. Nevertheless, I believe that this first-principles study in combination with Molecular Mechanics results serve as a key step towards understanding the role of surrounding residues for the translocation of copper in metallochaperones. It complements the NMR, X-ray and EXAFS experimental findings. I expect that these findings may be of use for understanding how copper or other metals bind to other metallochaperone proteins as well.

Acknowledgment. This work is supported in part by NIST Grant 70 NAMB 2H003 and DOE Grant DE-FG03-97ER45623, and was facilitated by the DOE Computational Materials Science Network. Computing was performed at NIST's Raritan cluster. I thank Dr. Zachary H. Levine (NIST) for his careful proofreading of the paper and continued support, and Prof. John J. Rehr and the members of his group at the University of Washington for helpful discussions. I thank Prof. I. Bertini and his collaborators for making the Cu(I)−Atx1 structure obtained by NMR available and J. E. Penner-Hahn, and T. V. O'Halloran for the XAFS data. The identification of any commercial product or trade name does not imply endorsement or recommendation by the National Institute of Standards and Technology

Supporting Information Available: Input file used in code FEFF for the computation of the EXAFS spectrum. Overlapping structures, Hg(II)−Atx1, Cu(I)−Atx1 reported using NMR spectroscopy and Cu(I)−Atx1 proposed in the present paper. Relaxed structure obtained using ONIOM-EE method in Brookhaven Protein Data Bank (PDB) format. This material is available free of charge via the Internet at http://pubs.acs.org.

References and Notes

(1) Solioz, M.; Vulpe, C. D. *Trends Biochem. Sci.* **1996**, *21*, 237.

(2) Silver, S.; Nucifora, G.; Chu, L.; Misra, T. K. *Trends Biochem. Sci.* **1989**, *14*, 76.

(3) Pufahl, R.; Singer, C. P.; Peariso, K. L.; Lin, S.-J.; Schmidt, P. J.; Fahrni, C. J.; Cizewski Culotta, V.; Penner-Hahn, J. E.; O'Halloran, T. V. *Science* **1997**, *278*, 853.

(4) Wakabayashi, T.; Nakamura, N.; Sambongi, Y.; Wada, Y.; Oka, T.; Futai, M. *FEBS Lett.* **1998**, *440*, 141.

(5) Banci, L.; Bertini, I.; Cantini, F.; Felli, I. C.; Gonnelli, L.; Hadjiliadis, N.; Pierattelli, R.; Rosato, A.; Voulgaris, P. *Nat. Chem. Biol.* **2006**, *2*, 367.

(6) Huffman, D. L.; O'Halloran, T. V. *J. Biol. Chem.* **2000**, *275*, 18611.

(7) Arnesano, F.; Banci, L.; Bertini, I.; Bonvin, A. M. J. J. *Structure* **2004**, *12*, 669.

(8) Rosenzweig, A. C.; Huffman, D. L.; Hou, M. Y.; Wernimont A. K.; Pufahl, R. A.; O'Halloran, T. V. *Structure* **1999**, *7*, 605.

(9) Banci, L.; Bertini, I.; Mangani, S. *J. Synchrotron Radiat.* **2005**, *12*, 94.

(10) Arnesano, F.; Banci, L.; Bertini, I.; Mangani, S.; Thompsett, A. T. *Proc. Natl. Assoc. Sci.* **2003**, *100*, 3814.

(11) Banci, L.; Bertini, I.; Baffoni, C.; Simone, D. L.; Huffman, T. V.; O'Halloran, T. V. *J. Biol. Chem.* **2001**, *275*, 8415. Banci, L.; Bertini, I.; DelConte, R.; Markley, J.; Ruiz-Duenas, F. J. *Biochemistry* **2001**, *40*, 15660. Banci, L.; Rosato, A. *Acc. Chem. Res.* **2003**, *36*, 215. Banci, L.; Bertini, I.; Ciofi-Baffoni, S.; D'Onofrio, M.; Gonnelli, L.; Marhuenda-Egea, C. F.; Ruiz-Duenas, F. J. *J. Mol . Biol.* **2002**, *317*, 415. Banci, L.; Bertini, I.; Ciofi-Baffoni, S.; Gonnelli, L.; Su, X. C. *J. Mol. Biol.* **2003**, *331*, 473. Arnesano, F.; Banci, L.; Bertini, I.; Cantini, F.; Ciofi-Baffoni, S.; Huffman, D. L.; O'Halloran, T. V. *J. Biol. Chem.* **2001**, *276*, 41365. Gitschier, J.; Moffat, B.; Reilly, D.; Wood, W. I.; Fairbrother, W. J. *Nat. Struct. Biol.* **1998**, *5*, 47. Wernimont, A. K.; Huffman, D. L.; Lamb, A. L.; O'Halloran, T. V.; Rosenzweig, A. C. *Nat. Struct. Biol.* **2000**, *7*, 766. Banci, L.; Bertini, I.; DelConte, R.; Mangani, S.; Meyer-Klaucke, W. *Biochemistry* **2003**, *42*, 2467.

(12) Arnesano, F.; Banci, L.; Bertini, I.; Huffman, D.; O'Halloran, T. V. *Biochemistry* **2001**, *40*, 1528.

(13) Ralle, M.; Lutsenko, S.; Blackburn, N. J. *J. Biol. Chem.* **2003**, *278*, 23163. Ralle, M.; Cooper, M. J.; Lutsenko, S.; Blackburn, N. J. *J. Am. Chem. Soc.* **1998**, *120*, 13525. DiDonato, M.; Hsu, H. F.; Narindrasorasak, S.; Que, L. J.; Sarkar, B. *Biochemistry* **2000**, *39*, 1890. Cobine, P. A.; George, G. N.; Winzor, D. J.; Harrison, M. D.; Mogahaddas, S.; Dameron, C. T. *Biochemistry* **2000**, *39*, 6857. Pickering, I. J.; George, G. N.; Dameron, C. T.; Kurz, B.; Winge, D. R.; Dance, I. G. *J. Am. Chem. Soc.* **1993**, *115*, 9498. Srinivasan, C.; Posewitz, M. C.; George, G. N.; Winge, D. R. *Biochemistry* **1998**, *37*, 7572. Heaton, D. N.; George, G. N.; Garrison, G.; Winge, D. R. *Biochemistry* **2001**, *40*, 743. Nittis, T.; George, G. N.; Winge, D. R. *J. Biol. Chem.* **2001**, *276*, 42520. Brown, K. R.; Keller, G. L.; Pickering, I. J.; Harris, H. H.; George, G. N.; Winge, D. R. *Biochemistry*

2002, *41*, 6469. Chen, K.; Yuldasheva, S.; Penner-Hahn, J. E.; O 'Halloran, T. V. *J. Am. Chem. Soc.* **2003**, *125*, 12088.

(14) Vreven, T.; Morokuma, K. *J. Comput. Chem.* **2000**, *16*, 1419. Vreven, T.; Byun, K. S.; Kommaroni, I.; Dapprich, S.; Montgomery, J. A.; Morokuma, K.; Frisch, M. J. *J. Chem. Theory Comput*. **2006**, *2*, 815.

(15) Warshel, A.; Levitt, M. *J. Mol. Biol.* **1976**, *106*, 421.

(16) Friesner, R.; Beachy, M. D. *Curr. Opin. Struct. Biol.* **1998**, *8*, 257.

(17) Vaidehi, N.; Wesolowski, T. A.; Warshel, A. *J. Chem. Phys.* **1992**, *97*, 4264.

(18) Vreven, T.; Morokuma, K. *J. Chem. Phys.* **2000**, *113*, 2969.

(19) Frisch, M. J. et al., Gaussian, Inc., Pittsburgh, PA.

(20) Maseras, M.; Morokuma, K. *J. Comput. Chem.* **1995**, *16*, 1170.

(21) Becke, A. D. *Phys. Rev. A.* **1988**, *38*, 3098. Becke, A. D. *J. Chem. Phys.* **1993**, *98*, 1372−1377. Becke, A. D. *J. Chem. Phys.* **1993**, *98*, 5648.

(22) Cornell, W. D.; Cieplak, P.; Bayly, C. I.; Gould, I. R.; Merz, K. M.; Ferguson, D. M.; Spellmeyer, D. C.; Fox, T.; Caldwell, J. W.; Kollman, P. A. *J. Am. Chem. Soc.* **1995**, *117*, 5179.

(23) In the current implementation of ONIOM-EE in gaussian03, it is not possible include an implicit solvent effect. The addition of an adequate number of water molecules is beyond the scope of this work.

(24) Besler, B. H.; Merz Jr., K. M.; Kollman, P. A. *J. Comput. Chem.* **1990**, *11*, 431.

(25) Comba, P. In *Molecular Modeling and Dynamics of Bioinorganic Systems*; Banci, L., Comba, P., Eds.; Kluwer Academic Publishers: P Dordrecht, The Netherlands, 1997; pp 21−47. Comba, P.; Remenyi, R. *J. Comput. Chem.* **2002**, *23*, 697.

(26) In the rigid limit, the copper atom is displaced along the bonds while the rest of the atoms are kept fixed.

(27) The anharmonic contribution was neglected in this work.

(28) MacKerell, A. D., Jr.; Bashford, D.; Bellott, R. L.; Dunbrack, R. L., Jr.; Evanseck, J. D.; Field, M. J.; Fischer, S.; Gao, J.; Guo, H.; Ha, S.; Joseph-McCarthy, D.; Kuchnir, L.; Kuczera, K.; Lau, F. T. K.; Mattos, C.; Michnick, S.; Ngo, T.; Nguyen, D. T.; Prodhom, B.; Reiher, W. E., III;, Roux, B.; Schlenkrich, M.; Smith, J. C.; Stote, R.; Straub, J.; Watanabe, M.; Wiorkiewicz-Kuczera, J.; Yin, D.; Karplus, M., A. D. *J. Phys. Chem. B* **1998**, *102*, 3586.

(29) Jorgensen, W. L.; Chandraseklar, J.; Madura, J. D.; Impey, R. W.; Klein, M. L. *J. Chem. Phys.* **1983**, *79*, 926.

(30) Ryckaert, J. P.; Ciccotti, G.; Berendsen, H. J. C. *J. Comput. Phys.* **1977**, *23*, 327.

(31) Hsiao, Ya-Wen; Ryde, U. *Inorg. Chim. Acta* **2006**, *359*, 1081.

(32) Poiarkova, A. N. X-ray Absorprion Spectroscopy Fine Structure Debye-Waller Factors. Ph.D. Thesis, University of Washington, Seattle, 1999.

(33) Rehr, J. J.; Kas, J. J.; Prange, M. P.; Vila, F. D.; Ankudinov, A. L.; Campbell, L. W.; Sorini, A. P. http://arxiv.org/abs/cond-mat/0601241 (accessed 2006).

(34) Rehr, J. J.; Mustre de Leon, J.; Zabinsky, S. I.; Albers, R. C. *J. Am. Chem. Soc.* **1991**, *113*, 5135. Mustre de Leon, J.; Rehr, J. J.; Zabinsky, S. I.; Albers, R. C. *Phys. Rev. B* **1991**, *44*, 4146.

(35) Rehr, J. J.; Albers, R. C. *Rev. Mod. Phys.* **2000**, *72*, 621.

(36) Heidin, L; Lundquist, S. *Solid State Physiscs: Advances in Research and Applications*; Academic: New York, 1969; Vol. 23.

(37) The reason why the equation-of-motion and the simple correlated model give similar results is due to the simple structure of the scattering center and the surrounding atoms.

(38) Cobine, P. A.; Winge, D. R. *Nat. Chem. Biol.* **2006**, *2*, 1.

(39) There is no correction for correlated displacement.

(40) Anastassopoulou, I.; Banci, L.; Bertini, I.; Cantini, F.; Katsari, E.; Rosato, A. *Biochemistry* **2004**, *43*, 13046

(41) Manas, E. S.; Getahun, Z.; Wright, W. W.; DeGrado, W. F.; Vanderkooi, J. M. *J. Am. Chem. Soc.* **2000**, *122*, 9883.

(42) Walsh, S. T. R.; Walsh, R.; Cheng, P.; Wright, W. W.; Daggett, V.; Vanderkooi, J. M.; DeGrado, W. F. *Protein Sci.* **2003**, *12*, 520.

(43) Fu, F. D.; DeOliveira, D. B.; Trumble, W. R.; Sarkar, H. K.; Singh, B. R. *Appl. Spectrosc.* **1994**, *48*, 1432.

(44) Jorgensen, W. L. *Science* **2004**, *303*, 1813.

(45) Ralle; M.; Lutsenko; S.; Blackburn, N. J. *J. Inorg. Biochem.* **2004**, *98*, 765.

(46) Cobine, P. A.; George, G. N.; Jones, C. E.; Wickramsinghe, W. A.; Solioz, M.; Dameron, C. T. *Biochemistry* **2002**, *41*, 5822.

(47) Pickering, I. J.; George, G. N.; Dameron, C. T.; Kurz, B.; Winge, D. R.; Dance, I. G. *J. Am. Chem. Soc.* **1993**, *115*, 9498.

(48) Kau, L. S.; Spira-Solomon, D.; Penner-Hahn, J. E.; Hodgson, K. O.; Solomon, E. I. *J. Am. Chem. Soc.* **1987**, *109*, 6422.

(49) Ungar, L. W.; Scherer, U. F.; Voth, G. A. *Biophys. J.* **1997**, *72*, 5.